

## Facile characterization of ripple domains on exfoliated graphene

Jin Sik Choi, Jin-Soo Kim, Ik-Su Byun, Duk Hyun Lee, In Rok Hwang et al.

Citation: *Rev. Sci. Instrum.* **83**, 073905 (2012); doi: 10.1063/1.4737428

View online: <http://dx.doi.org/10.1063/1.4737428>

View Table of Contents: <http://rsi.aip.org/resource/1/RSINAK/v83/i7>

Published by the [American Institute of Physics](#).

---

### Related Articles

Improved memory characteristics by NH<sub>3</sub>-nitrided GdO as charge storage layer for nonvolatile memory applications

*Appl. Phys. Lett.* **101**, 033501 (2012)

Mn-activated K<sub>2</sub>ZrF<sub>6</sub> and Na<sub>2</sub>ZrF<sub>6</sub> phosphors: Sharp red and oscillatory blue-green emissions

*J. Appl. Phys.* **112**, 013506 (2012)

Fabrication of binary FeSe superconducting wires by diffusion process

*J. Appl. Phys.* **111**, 112620 (2012)

Versatile system for the temperature-controlled preparation of oxide crystal surfaces

*Rev. Sci. Instrum.* **83**, 055110 (2012)

In situ microwave characterization of microwire composites with external magnetic field

*Appl. Phys. Lett.* **100**, 192903 (2012)

---

### Additional information on *Rev. Sci. Instrum.*

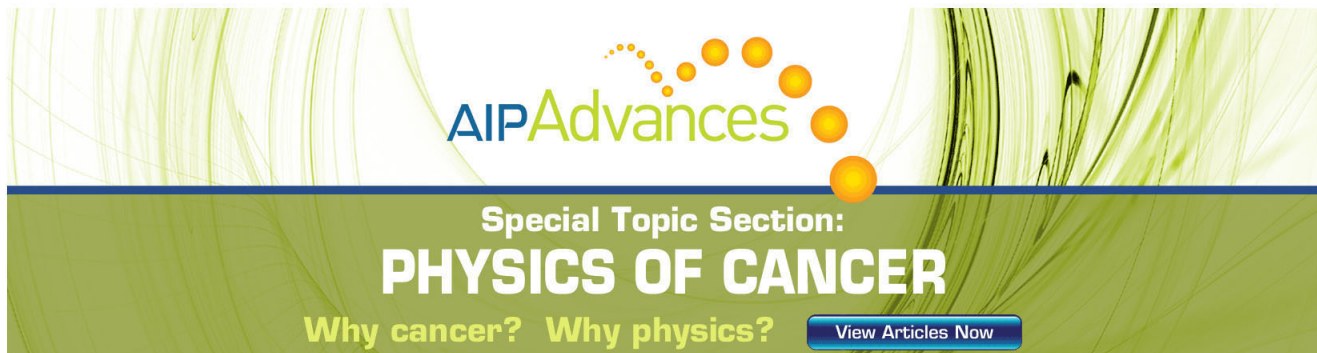
Journal Homepage: <http://rsi.aip.org>

Journal Information: [http://rsi.aip.org/about/about\\_the\\_journal](http://rsi.aip.org/about/about_the_journal)

Top downloads: [http://rsi.aip.org/features/most\\_downloaded](http://rsi.aip.org/features/most_downloaded)

Information for Authors: <http://rsi.aip.org/authors>

## ADVERTISEMENT



**AIP Advances**

Special Topic Section:  
**PHYSICS OF CANCER**

Why cancer? Why physics? [View Articles Now](#)

## Facile characterization of ripple domains on exfoliated graphene

Jin Sik Choi,<sup>1</sup> Jin-Soo Kim,<sup>1</sup> Ik-Su Byun,<sup>1</sup> Duk Hyun Lee,<sup>1</sup> In Rok Hwang,<sup>1</sup>  
Bae Ho Park,<sup>1,a)</sup> Taekjib Choi,<sup>2</sup> Jeong Young Park,<sup>3,a)</sup> and Miquel Salmeron<sup>4</sup>

<sup>1</sup>*Division of Quantum Phases and Devices, Department of Physics, Konkuk University,  
Seoul 143-701, South Korea*

<sup>2</sup>*HMC and INAME, Faculty of Nanotechnology and Advanced Materials Engineering, Sejong University,  
Seoul 143-747, South Korea*

<sup>3</sup>*Graduate School of Energy, Environment, Water, and Sustainability, NanoCentury KI, Korea Advanced  
Institute of Science and Technology, Daejeon 305-701, South Korea*

<sup>4</sup>*Materials Science Division, Lawrence Berkeley National Laboratory, Berkeley, California 94720, USA*

(Received 15 March 2012; accepted 26 June 2012; published online 26 July 2012)

Ripples in graphene monolayers deposited on SiO<sub>2</sub>/Si wafer substrates were recently shown to give rise to friction anisotropy. High friction appears when the AFM tip slides in a direction perpendicular to the ripple crests and low friction when parallel. The direction of the ripple crest is, however, hard to determine as it is not visible in topographic images and requires elaborate measurements of friction as a function of angle. Here we report a simple method to characterize ripple crests by measuring the cantilever torsion signal while scanning in the non-conventional longitudinal direction (i.e., along the cantilever axis, as opposed to the usual friction measurement). The longitudinal torsion signal provides a much clearer ripple domain contrast than the conventional friction signal, while both signals show respective rotation angle dependences that can be explained using the torsion component of the normal reaction force exerted by the graphene ripples. We can also determine the ripple direction by comparing the contrast in torsion images obtained in longitudinal and lateral scans without sample rotation or complicated normalization. © 2012 American Institute of Physics. [<http://dx.doi.org/10.1063/1.4737428>]

### I. INTRODUCTION

Recently, frictional studies on low dimensional materials, such as carbon nanotubes (CNT),<sup>1</sup> graphene,<sup>2-5</sup> and organic monolayers,<sup>6-13</sup> have attracted much interest. Since these low dimensional materials are soft, they are prone to structural deformation during the fabrication process. Symmetry breaking induced by structural deformation may lead to the deterioration of electrical or electro-mechanical performance for low dimensional materials due to the extremely high surface-to-volume ratios and strong crystallographic dependence of their physical properties. Recent studies revealed that characteristic ripple structures were usually formed in supported<sup>13-18</sup> and suspended graphene samples.<sup>19-21</sup> We have shown this in a recent study of the friction properties of exfoliated graphene deposited on a SiO<sub>2</sub> substrate, where we discovered the existence of anisotropic friction domains with a 180° period by measuring the torsion of the AFM cantilever ( $T_{LAT}$ ) during lateral scanning of a tip attached to the cantilever. We explained the finding as a result of stress-induced ripples created by inhomogeneous contact of the graphene sheet with the substrate. The ripples give rise to anisotropic torsion on the cantilever during AFM tip scanning, where the highest friction occurs when the tip slides in a direction perpendicular to the ripple crests and lowest when it scans in the parallel direction. We also showed that the ripple domains could be removed by heating the substrate, which then made the graphene friction homogeneous. To determine the ripple di-

rection of each domain, the friction force was measured as a function of scanning angle after incrementally rotating the sample. This process requires the AFM tip to be retracted and brought back into contact for each rotation angle, thus requiring complicated normalization.<sup>2</sup>

In this paper, we report that the ripple structures on monolayer graphene can be more effectively characterized by measuring cantilever torsion while scanning in the longitudinal direction ( $T_{LON}$ ), i.e., along the cantilever arm, as opposed to conventional scanning in the perpendicular direction. Although a similar method has been used to determine grain orientation in polycrystalline organic semiconductors,<sup>11-13</sup> ripple structures on graphene have not been characterized by  $T_{LON}$ , which produces a much clearer domain contrast than images of  $T_{LAT}$ . Both normalized  $T_{LON}$  and  $T_{LAT}$  show rotation angle dependences that can be explained using the torsional component of the normal reaction force exerted by the graphene ripples. We can also determine the ripple direction on each domain by comparing the domains of both  $T_{LON}$  and  $T_{LAT}$  images, without the need for measuring complicated sample rotation angle dependence.

### II. EXPERIMENTAL DETAILS

#### A. Sample preparation and AFM measurement conditions

Graphene flakes were deposited, using the standard mechanical exfoliation method, onto thermally grown silicon dioxide (SiO<sub>2</sub>: 300 nm) substrates at ambient conditions without any further treatment. The thin graphene samples were sorted using optical microscopy. The number of graphene

<sup>a)</sup>Authors to whom correspondence should be addressed. Electronic addresses: baehpark@konkuk.ac.kr and jeongyupark@kaist.ac.kr.

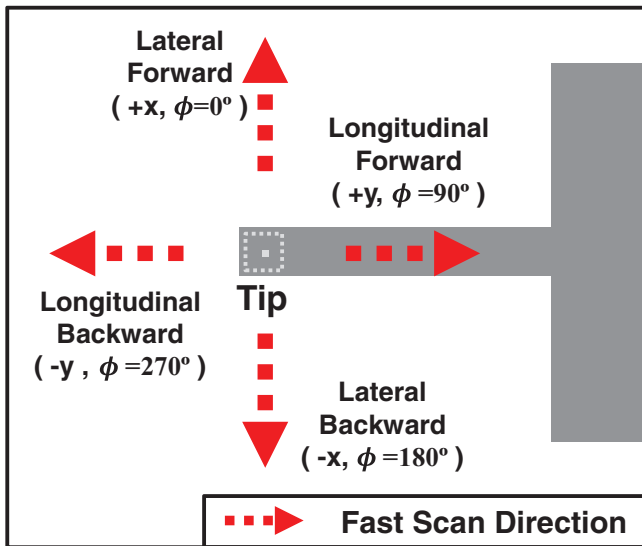


FIG. 1. General definition of scan direction relative to the cantilever body (top view).

layers was confirmed by Raman spectroscopy, with the 514.5-nm laser line of an  $\text{Ar}^+$ -ion laser used as an excitation source.

AFM topography and torsion images were simultaneously obtained in contact mode with a Seiko SPA-300HV AFM at ambient conditions. During these measurements, the loading force (0 nN) was kept fixed. We used silicon AFM tips (nanosensors PPP-LFMR with a spring constant of 0.2 N/m) for imaging. The topographic images were pro-

cessed by line and plane subtraction corrections to compensate for scanning drift. The scan directions of the torsion images were parallel ( $\phi = 90^\circ$  for forward and  $270^\circ$  for backward) or perpendicular ( $\phi = 0^\circ$  for forward and  $180^\circ$  for backward) to the cantilever axis. Torsion domain images were observed reproducibly in isolated monolayer graphene samples of various sizes and shapes, which were fabricated as described above. We obtained these results with various tips, including silicon and silicon nitride-coated tips with a low spring constant to maintain torsion measurement sensitivity. Furthermore, the results can be observed with a couple of AFM systems (Seiko SPA-300HV and PSIA XE-100).

## B. General definition of scan direction

We have followed the general definition of scan direction, as shown in Fig. 1. Longitudinal and lateral scans are carried out along the  $\pm y$ - and  $\pm x$ -directions, respectively. The positive and negative signs imply forward and backward scans, respectively. Each scan direction can be designated using a rotation angle  $\phi$  of scan direction (clockwise) from the  $+x$ -direction. In this paper, all images are aligned to this fixed cantilever direction.

## III. RESULTS AND DISCUSSION

### A. Longitudinal and lateral torsion images

Figures 2(a) and 2(b) show the images of  $T_{\text{LON}}$  and  $T_{\text{LAT}}$ , obtained simultaneously after incrementally rotating the

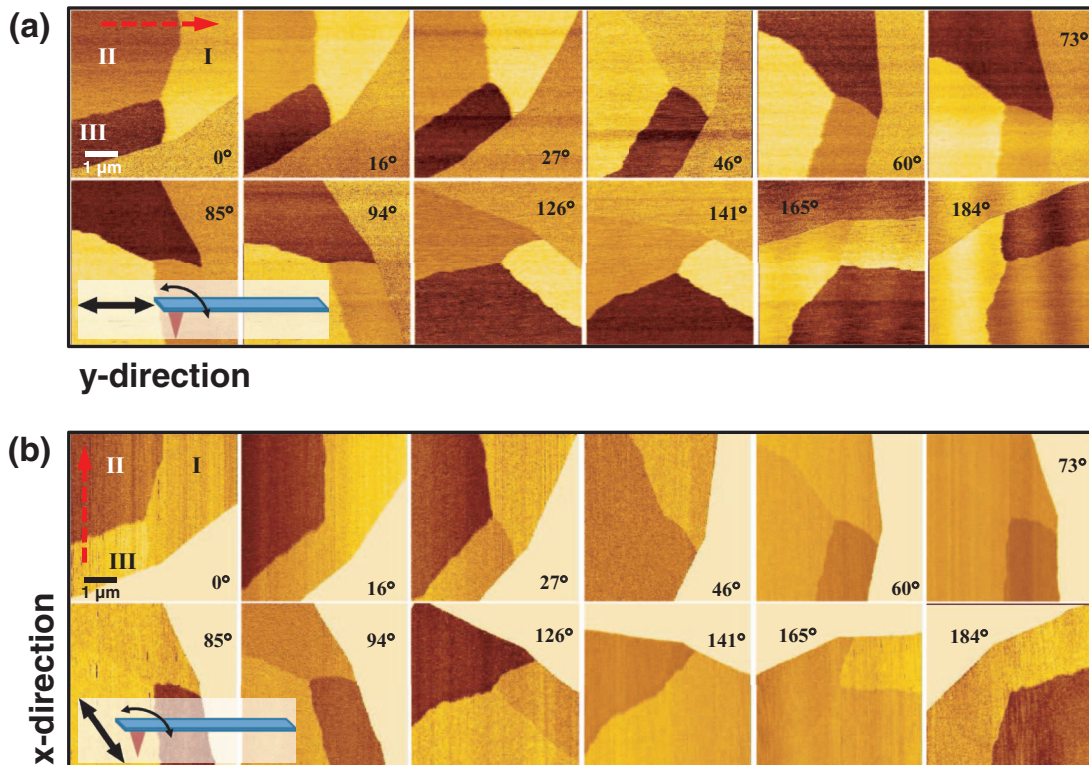


FIG. 2. Images of the cantilever torsion measured during (a) scans parallel to the cantilever arm direction (longitudinal,  $T_{\text{LON}}$ ), and (b) scans perpendicular to the cantilever arm (lateral,  $T_{\text{LAT}}$ ). From left to right, the  $\text{SiO}_2$  substrate supporting the graphene layer is rotated counterclockwise. The red dashed arrow indicates the AFM tip scanning direction during each measurement. (Part (b) is the same as Fig. 2(a) in Ref. 2 and is used for comparison. Reprinted with permission from J. S. Choi, J.-S. Kim, I.-S. Byun, D. H. Lee, M. J. Lee, B. H. Park, C. Lee, D. Yoon, H. Cheong, K. H. Lee, Y.-W. Son, J. Y. Park, and M. Salmeron, *Science* **333**, 607 (2011). Copyright 2011 AAAS.)



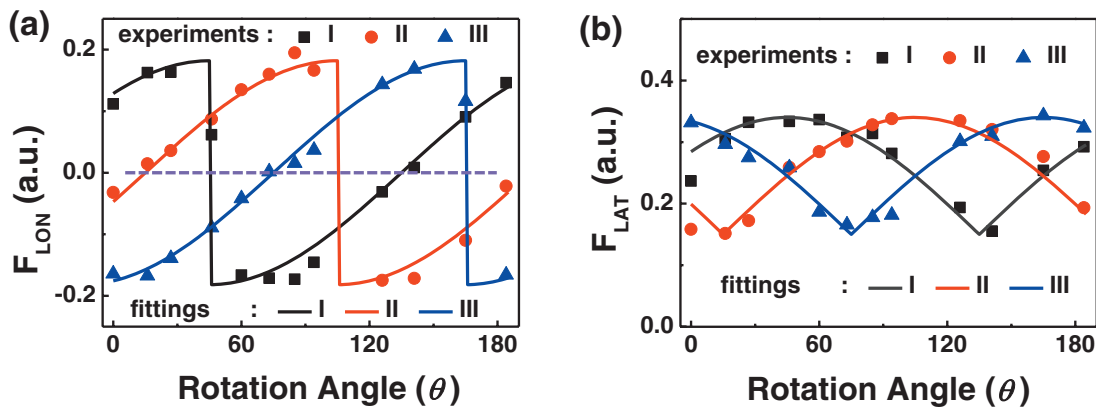


FIG. 3. Dependence of the normalized torsion on sample rotation angle when the AFM tip scans the surface along the (a) longitudinal ( $F_{LON}$ ) and (b) lateral ( $F_{LAT}$ ) directions. (Part (b) is the same as Fig. 2(b) in Ref. 2 and is used for comparison. Reprinted with permission from J. S. Choi, J.-S. Kim, I.-S. Byun, D. H. Lee, M. J. Lee, B. H. Park, C. Lee, D. Yoon, H. Cheong, K. H. Lee, Y.-W. Son, J. Y. Park, and M. Salmeron, *Science* **333**, 607 (2011). Copyright 2011 AAAS.)

sample while keeping the scan direction parallel (y-direction;  $\phi = 90^\circ$ ) and perpendicular (x-direction;  $\phi = 0^\circ$ ) to the cantilever body direction, respectively. In both the scanning directions, the images show that the graphene monolayer consists of three frictional domains. It is noteworthy that while each image in Fig. 2(a) shows three domains with different contrast, several neighboring domains in the images in

Fig. 2(b) (the standard friction image) exhibit the same contrast. Moreover, the contrast in the longitudinal scans is clearer than in the lateral scans. Since the friction domains are the result of ripples in the graphene, it is clear that the ripples affect both  $T_{LON}$  and  $T_{LAT}$ , but in different ways, depending on the angle between the cantilever body and the direction of the ripple crests. These results are contrary to those

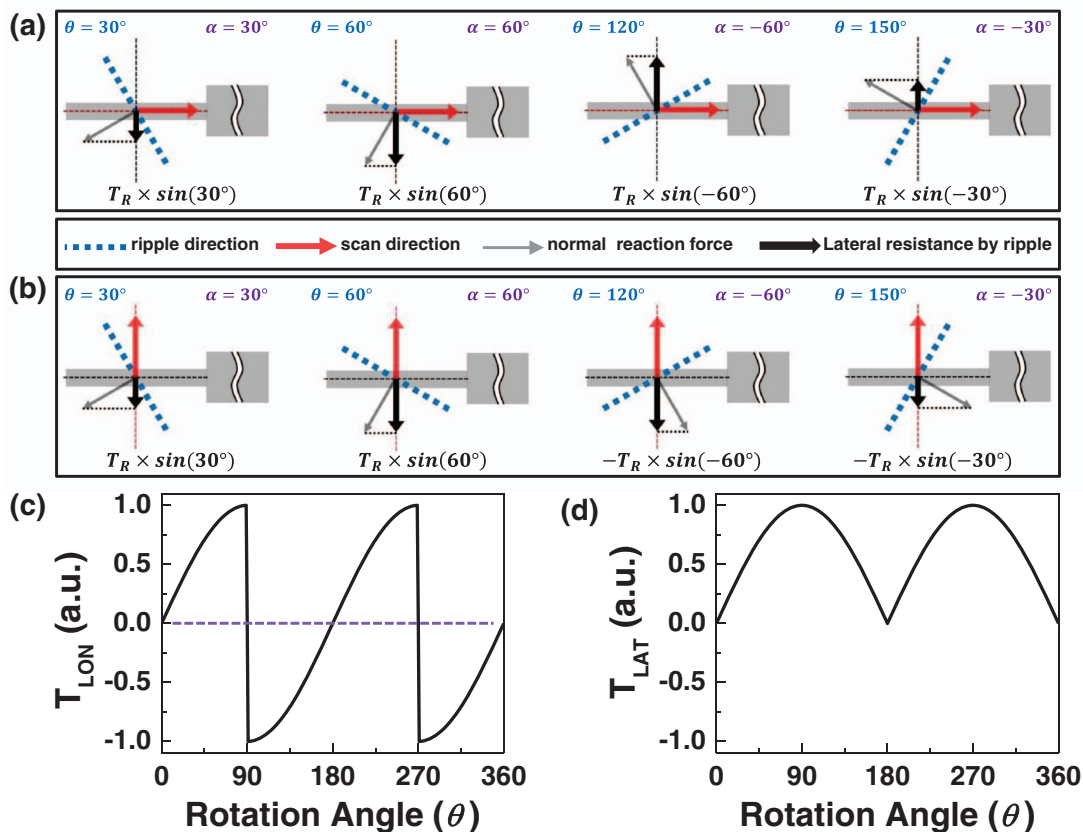


FIG. 4. Schematic diagrams for the in-plane direction of ripples (blue broken line) on graphene, cantilever scan, the normal reaction force exerted by the ripple, and torsion on the cantilever body during (a) longitudinal and (b) lateral scans at several sample rotation angles. The resultant sample rotation angle dependence of the cantilever torsion during (c) longitudinal, and (d) lateral scans.  $\theta$  is the sample rotation angle (counter-clockwise) and  $\alpha$  is the rotation angle of the nearest ripple (counter-clockwise) from the  $x$ -direction ( $\Phi = 0^\circ$ ).  $T_R$  is the amplitude of the normal reaction force exerted by ripples.

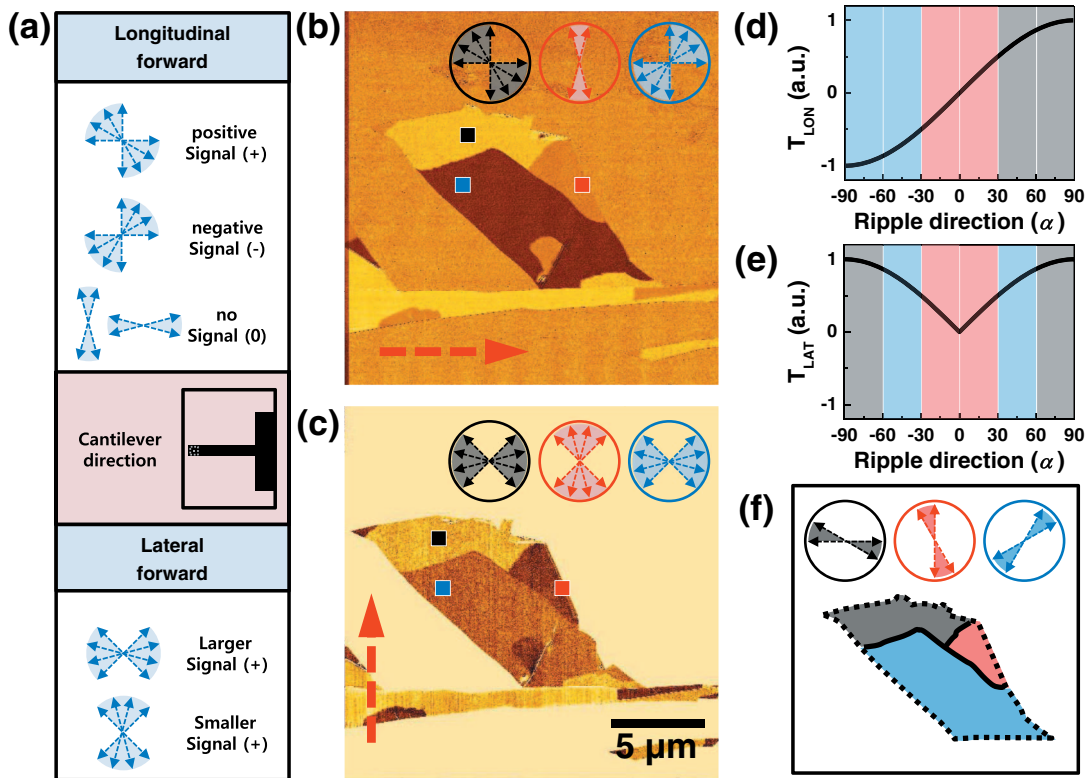


FIG. 5. (a) The relationship between ripple direction and cantilever torsion during longitudinal and lateral scans. (b) Longitudinal and (c) lateral scan torsion images obtained on a graphene sample. The torsion images are obtained by subtracting torsion values in the positive and negative scan directions. The calculated ripple direction dependence of (d)  $T_{LON}$  and (e)  $T_{LAT}$ . The shaded area exhibits the possible ripple directions of domains denoted by corresponding colors in (b) and (c). (f) Resultant ripple direction ranges determined by comparing longitudinal and lateral scan torsion images.

found in the case of polycrystalline organic semiconductor films whose grain orientation significantly affected  $T_{LON}$ , but not  $T_{LAT}$ .<sup>11–13</sup>

## B. Normalized longitudinal and lateral friction signals

We have observed that the  $T_{LAT}$  of isotropic  $\text{SiO}_2$  varies while measuring dependence on sample rotation angle since we cannot maintain exactly the same loading conditions, which significantly affect  $T_{LAT}$ . In order to remove such extrinsic effects and quantitatively compare the angular dependence of  $T_{LON}$  and  $T_{LAT}$ , we normalized the torsional response, as follows. At each sample rotation angle, four different cantilever torsion values were measured corresponding to the AFM tip scanning along the positive and negative  $y$ -, and positive and negative  $x$ -directions. The normalized signal ( $F_{LAT}$ ) of  $T_{LAT}$  was obtained by subtracting the signals of the positive and negative scans in each domain, and dividing this value by the corresponding signal of the surrounding  $\text{SiO}_2$  area, which is independent of rotation angle. In the case of the normalized signal ( $F_{LON}$ ) of  $T_{LON}$ , the difference between the  $T_{LON}$  signals obtained from the positive and negative scans for each domain and rotation angle is divided by the difference between the  $T_{LAT}$  signals of  $\text{SiO}_2$  from the positive and negative scans. Our technique is beneficial in characterizing anisotropic deformations of other low dimensional materials when an isotropic reference material is simultaneously investigated.

Figures 3(a) and 3(b) show the sample rotation angle dependence of  $F_{LON}$  and  $F_{LAT}$ , respectively. The minimum value represents the contribution from the isotropic energy dissipation, except for the presence of ripples that induce additional anisotropic energy dissipation. The angle dependence of  $F_{LON}$  at each domain in Fig. 3(a) shows a  $180^\circ$  period, with each domain shifted by  $60^\circ$  with respect to each other, as in the  $F_{LAT}$  case. Note that the difference between the maximum and the minimum  $F_{LON}$  ( $0.38 \pm 0.01$ ) is twice as large as that of  $F_{LAT}$  ( $0.19 \pm 0.01$ ). Moreover, unlike  $F_{LAT}$ , which changes values but always remains positive,  $F_{LON}$  oscillates from positive to negative values with zero as the average, thus providing a more sensitive characterization contrast for the presence of ripple structures.

## C. Interactions between the cantilever and ripples during longitudinal and lateral scans

In order to understand these phenomena, we consider each domain with its characteristic ripple direction. As the tip pushes the ripple crest, it feels the in-plane reaction force exerted by the ripple, which bends the cantilever, as shown in Figs. 4(a) and 4(b). The reaction force exerted by the ripple does not depend on the angle between the cantilever and the ripple crest direction. Therefore, the torsions on the cantilever body during longitudinal and lateral scans have a  $\sin \alpha$  dependence, where  $\alpha$  is the rotation angle of the nearest ripple (counter-clockwise) from the  $x$ -direction ( $\phi = 0^\circ$ ). If

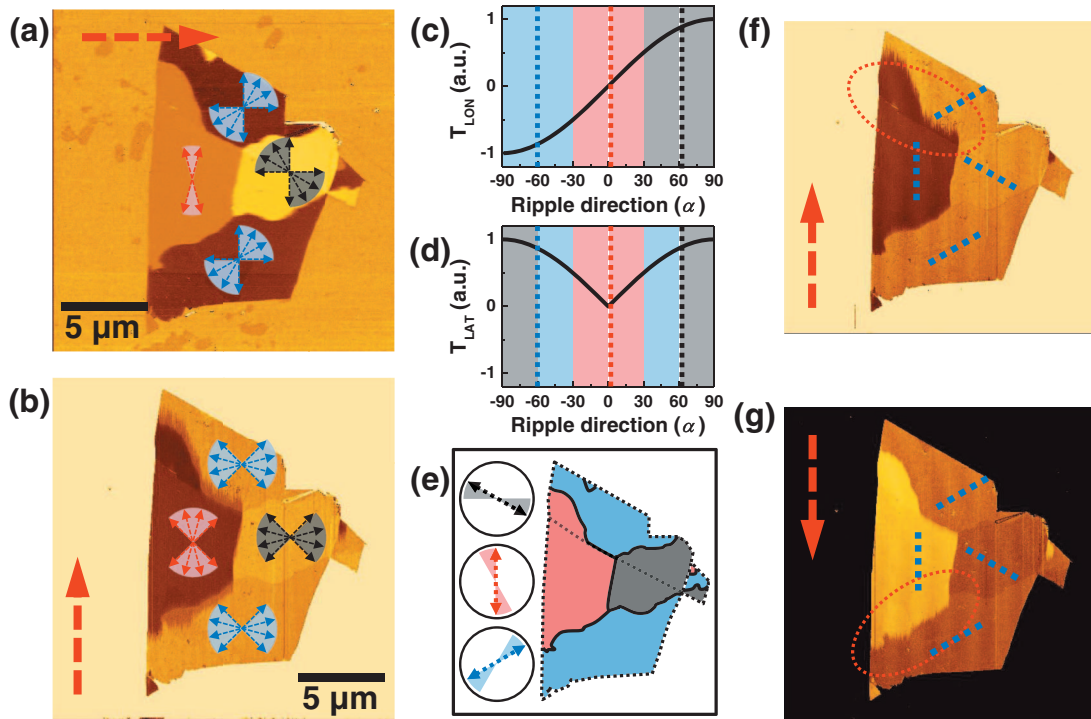


FIG. 6. (a) Longitudinal and (b) lateral scan torsion images obtained on a graphene sample. The calculated ripple direction dependence of (c)  $T_{LON}$  and (d)  $T_{LAT}$ . (e) Resultant ripple direction ranges determined by comparing longitudinal and lateral scan torsion images. The lateral torsion images obtained during (f) positive and (g) negative directional scans. The torsion image of (b) is obtained by subtracting torsion values in the positive (f) and negative (g) scan directions. The blurred domain boundaries are visible in the circled region.

the ripple in domain  $i$  has an initial rotation angle  $\theta_i$  from the  $x$ -direction and  $\theta$  is the sample rotation angle (counter-clockwise), the same  $\sin \alpha$  dependences are kept where  $\alpha = \theta + \theta_i - 180^\circ \times n$  ( $n$  is an integer) and  $-90^\circ \leq \alpha \leq 90^\circ$ .

During both longitudinal and lateral scans, the ripple structure can induce torsion on the cantilever body. Therefore,  $T_{LON}$  and  $T_{LAT}$  induced by ripple structures show  $\sin \alpha$  and  $|\sin \alpha|$  dependence, as shown in Figs. 4(c) and 4(d), respectively, in agreement with the experimental normalized data in Figs. 3(a) and 3(b). Fitting  $T_{LON}$  and  $T_{LAT}$  to a  $\sin \alpha$  function supports our reasoning that the in-plane reaction force exerted by a ripple does not depend on the angle between the cantilever and the ripple. The  $60^\circ$  shift of the data obtained for each neighboring domain reflects the fact that the ripples in one domain are rotated by  $60^\circ$  with respect to those in the neighboring domain. This in turn indicates that the ripple directions are related to the crystallographic directions of the graphene lattice where bending the graphene is easier, like the armchair or zigzag directions.

If we consider the scan direction dependence of the cantilever torsion due to the additional force exerted by a ripple,  $\alpha_i = \theta_i - 180^\circ \times n$  ( $n$  is an integer) is fixed and the cantilever torsion will be expressed by the following simple equations:

$$T_R \times \sin(\alpha_i), \text{ when } 0^\circ < (\phi + \alpha_i) < 180^\circ, \quad (1)$$

$$-T_R \times \sin(\alpha_i), \text{ when } 180^\circ < (\phi + \alpha_i) < 360^\circ, \quad (2)$$

where  $\phi$  is the rotation angle of the scan-direction from the  $x$ -direction (clockwise) and  $-\alpha_i < \phi < -\alpha_i + 360^\circ$ .

#### D. Determination of ripple direction without sample rotation

We can determine ripple direction using images of cantilever torsion without sample rotation and normalization. As shown in Fig. 5(a), the longitudinal scan torsion can determine whether the ripple is rotated in the clockwise or counter-clockwise direction from the  $y$ -axis, and the lateral scan torsion can distinguish whether the ripple direction is close to the  $x$ - or  $y$ -axis. Moreover, we can argue that ripple direction is very close to the  $x$ - or  $y$ -axis when the contrast of the longitudinal scan torsion is the same as the isotropic bulk  $\text{SiO}_2$ , which provides negligible longitudinal scan torsion. Therefore, from the longitudinal and lateral scan torsion images in Figs. 5(b) and 5(c), we can infer the ripple direction of each domain, as shown in the upper circular insets of Figs. 5(b) and 5(c). By comparing these data, we can determine the ripple direction of each domain in the  $45^\circ$  range.

Moreover, by considering that the angle dependence of torsion at each domain shows a  $60^\circ$  shift with respect to that of a neighboring domain, we can reduce the range of the ripple direction. Figures 5(d) and 5(e) show the theoretical ripple direction dependence of  $T_{LON}$  and  $T_{LAT}$ , respectively. Due to the  $60^\circ$  shift of ripples on neighboring domains, the bright (black), medium (red), and dark (blue) domains in Fig. 5(b) have ranges of  $\alpha$  between  $30^\circ$  and  $90^\circ$ , between  $-30^\circ$  and  $30^\circ$ , and between  $-90^\circ$  and  $-30^\circ$ , respectively, as shown in Fig. 5(d). Similarly, the bright (black), medium (blue), and dark (red) domains in Fig. 5(c) have ranges of  $\alpha$  between  $-90^\circ$  and  $-60^\circ$  or  $60^\circ$  and  $90^\circ$ , between  $-60^\circ$  and  $-30^\circ$  or  $30^\circ$  and  $60^\circ$ , and between  $-30^\circ$  and  $30^\circ$ ,

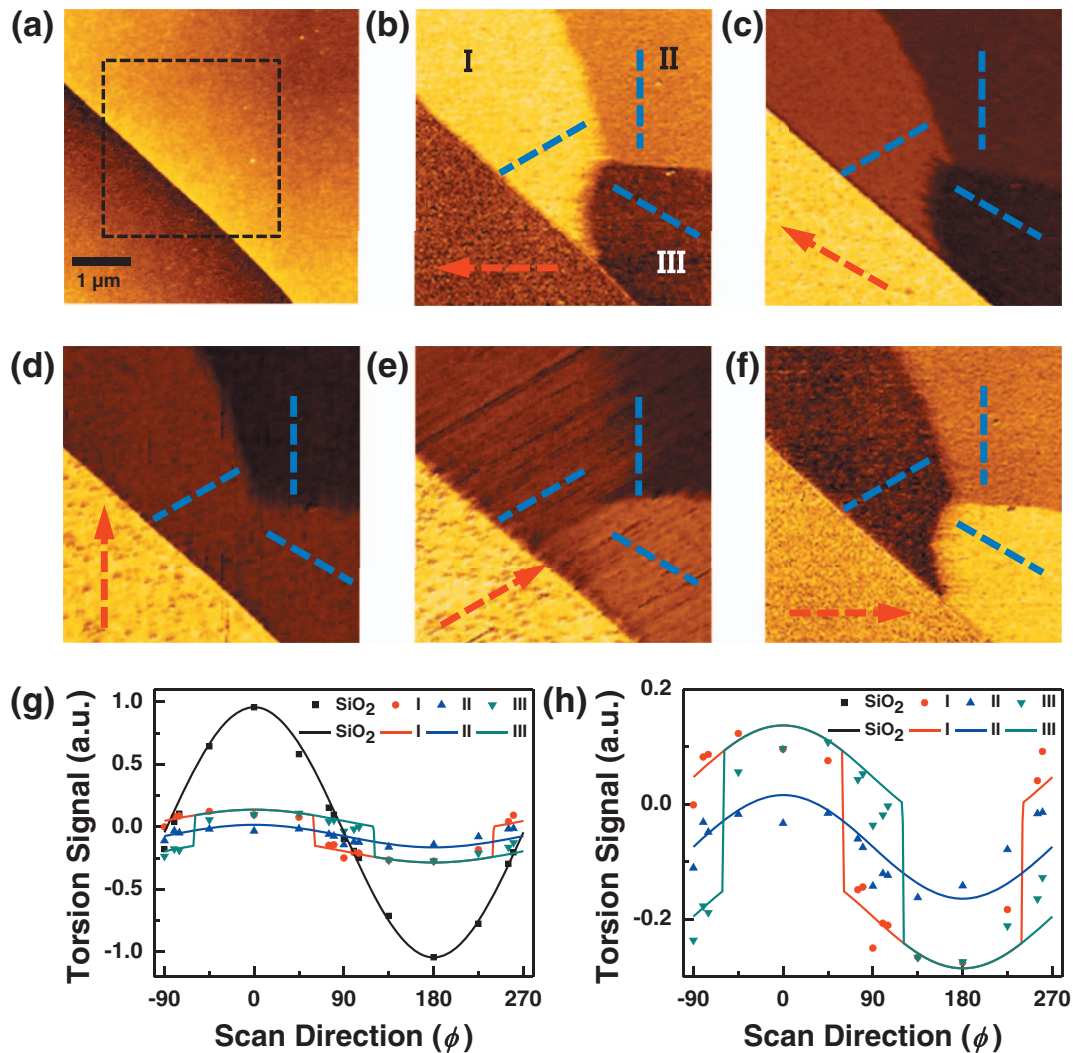


FIG. 7. (a) Topographic image, and scan direction dependence of (b)–(f) torsion images and (g) and (h) signals for monolayer graphene on  $\text{SiO}_2$ . The red dashed arrow and blue dashed line denote the fast scan and ripple directions at each domain, respectively.

respectively, as shown in Fig. 5(e). Then, we can determine the ripple directions in  $30^\circ$  ranges, as shown in Fig. 5(f), from the overlapped regions of Figs. 5(d) and 5(e), which are obtained by longitudinal and lateral scan torsion images. The results indicate that by employing both longitudinal and lateral scans on the exfoliated graphene, it is possible to determine the direction of ripples without sample rotation. More generally, this technique can be used to elucidate the direction of friction anisotropy on mechanically anisotropic regions of low dimensional materials.

### E. Blurred domain boundary in a torsion image

We can determine the ripple direction in  $30^\circ$  ranges on another graphene sample by comparing the longitudinal and lateral scan torsion images, as shown in Figs. 6(a)–6(e). Interestingly, we can find some blurred domain boundaries in Fig. 6(b) while they are not found in Fig. 6(a). If we compare the scan directions of Figs. 6(a) and 6(b), we notice that the blurred domain boundary is observed when the tip slides from the region where scan direction is the same as the ripple

direction of the domain to other regions. The blurring is associated with mechanical instability of the tip-sample junction when the tip slides from the slippery domain (where the ripple is parallel to the scan direction) to the high friction domain. Figures 6(f) and 6(g) reveal that the lateral scan from the red domain designated in Fig. 6(e) to another domain results in the blurred domain boundary. Therefore, we can argue that the ripple direction of the red domain is parallel to the scan direction. It also means that the blurred domain boundary can help us determine the ripple direction of the adjacent domain more precisely. We can then assign the ripple direction of each domain using the  $60^\circ$  shift in the ripple direction on the neighboring domains. The combination of lateral and longitudinal scans gives rise to facile determination of ripple direction on the graphene surface, with the potential application of unraveling mechanically anisotropic materials.

### F. Scan direction dependence

We also measured the scan direction ( $\phi$ ) dependence at a fixed sample rotation angle. This experiment was



performed in a high-vacuum environment ( $\sim 10^{-4}$  torr). Figure 7(a) shows the topography of monolayer graphene on a SiO<sub>2</sub> substrate. We measured the scan direction dependence of the torsion image (Figs. 7(b)–7(f)) in the black dashed rectangle area in Fig. 7(a). We can clearly observe three torsion domains that reveal different colors, depending on scan direction. Figure 7(g) shows the scan direction dependence of the torsion signal divided by the maximum torsion value of SiO<sub>2</sub> without subtracting the signals of the positive and negative scans. Figure 7(h) exhibits an expansion of Fig. 7(g) for a detailed comparison of torsion signals in the graphene domains. The torsion signal of the SiO<sub>2</sub> substrate shows a simple  $\cos\phi$  dependence, which is expected for a two-dimensionally isotropic material. The torsion signal of graphene may result from both the hard bulk surface, like graphite, and soft ripple deformation. The torsion signal from the hard bulk surface may show simple  $\cos\phi$  dependence, while that from soft ripple deformation may show a constant value of  $\pm T_R \times \sin(\alpha_i)$ , as described in Eqs. (1) and (2). Therefore, we can fit the experimental data, as shown in Figs. 7(g) and 7(h), using  $F_B \cos\phi \pm T_R \times \sin(\alpha_i)$ , where  $F_B$  is the maximum torsion signal from the hard bulk surface. It is estimated that  $F_B = 0.09$ ,  $T_R = 0.14$ , and  $\alpha_{i_I}$ ,  $\alpha_{i_{II}}$ , and  $\alpha_{i_{III}}$  are  $-60^\circ$ ,  $0^\circ$ , and  $60^\circ$ , respectively. The ripple direction of each domain is determined by these fitting results. Furthermore, we can find blurred domain boundaries and confirm that they provide useful information on the ripple directions of the adjacent domains (Fig. 7(c)–7(e)), as described in Sec. III E. From the fitting results in Fig. 7(h), we confirm that including the contribution from ripples leads to a better fit of the experimental scan directional dependence, except at any abruptly changing points where the scan and ripple directions are parallel.

#### IV. SUMMARY

In conclusion, the cantilever torsion obtained in a longitudinal scan provides a facile method to characterize the anisotropic ripple structure on monolayer graphene. The torsion signal in longitudinal scanning on exfoliated monolayer graphene has not been predicted and tried before, while the torsion signal in lateral scan has been investigated for characterizing surface friction of graphene. It produces a much clearer domain contrast, probably resulting from different ripple directions, than images of the torsion signal in lateral scan. The observed anisotropic torsion signal in the longitudinal scan can be additional experimental evidence for the existence of the ripple crests on monolayer graphene. Moreover, we can determine the ripple direction in each domain by obtaining torsion images in both longitudinal and lateral scans without performing complicated sample rotation experiments. This technique is applicable to characterize anisotropic deformations on low dimensional materials, such as self-assembled monolayers.

#### ACKNOWLEDGMENTS

This work was supported by National Research Laboratory (NRL) Program (Grant No. 2008-0060004), World Class University (WCU) Program (Grant No. R31-2008-000-10057-0), Nano-Material Technology Development Program (Grant No. 2011-0030228), and Quantum Metamaterials Research Center (Grant No. R11-2008-053-03002-0) through the NRF funded by the Korea government Ministry of Education, Science and Technology (MEST), and Seoul R&BD Program (Grant No. WR090671). J.Y.P. acknowledges support by WCU (World Class University) program (R-31-2008-000-10055-0), KRF-2010-0005390, and SRC Centre for Topological Matter (Grant No. 2011-0030787) through the National Research Foundation (NRF) of Korea funded by the Ministry of Education, Science and Technology (MEST) of Korea. M.S. was supported by the Office of Basic Energy Sciences, Division of Materials Sciences and Engineering of the U.S. Department of Energy under Contract No. DE-AC02-05CH11231.

- <sup>1</sup>M. Lucas, X. Zhang, I. Palaci, C. Klinke, E. Tosatti, and E. Riedo, *Nature Mater.* **8**, 876 (2009).
- <sup>2</sup>J. S. Choi, J.-S. Kim, I.-S. Byun, D. H. Lee, M. J. Lee, B. H. Park, C. Lee, D. Yoon, H. Cheong, K. H. Lee, Y.-W. Son, J. Y. Park, and M. Salmeron, *Science* **333**, 607 (2011).
- <sup>3</sup>C. Lee, Q. Li, W. Kalb, X. Liu, H. Berger, R. W. Carpick, and J. Hone, *Science* **328**, 76 (2010).
- <sup>4</sup>T. Filleter, J. L. McChesney, A. Bostwick, E. Rotenberg, K. V. Emtsev, Th. Seyller, K. Hom, and R. Bennewitz, *Phys. Rev. Lett.* **102**, 086102 (2009).
- <sup>5</sup>H. Lee, N. Lee, Y. Seo, J. Eom, and S. W. Lee, *Nanotechnology* **20**, 325701 (2009).
- <sup>6</sup>R. W. Carpick, D. Y. Sasaki, and A. R. Burns, *Tribol. Lett.* **7**, 79 (1999).
- <sup>7</sup>M. Liley, D. Gourdon, D. Stamou, U. Meseth, T. M. Fischer, C. Lautz, H. Stahlberg, H. Vogel, N. A. Burnham, and C. Duschl, *Science* **280**, 273 (1998).
- <sup>8</sup>H. Schönherr, P. J. A. Kenis, J. F. J. Engbersen, S. Harkema, R. Hulst, D. N. Reinhoudt, and G. J. Vancso, *Langmuir* **14**, 2801 (1998).
- <sup>9</sup>T. Ohzono and M. Fujihira, *Tribol. Lett.* **9**, 63 (2000).
- <sup>10</sup>J. Chen, I. Ratera, A. Murphy, D. F. Ogletree, J. M. J. Fréchet, and M. Salmeron, *Surf. Sci.* **600**, 4008 (2006).
- <sup>11</sup>M. Campione and E. Fumagalli, *Phys. Rev. Lett.* **105**, 166103 (2010).
- <sup>12</sup>V. Kalihari, E. B. Tadmor, G. Haugstad, and C. D. Frisbie, *Adv. Mater.* **20**, 4033 (2008).
- <sup>13</sup>H.-G. Flesch, S. G. J. Mathijssen, F. Gholamrezaie, A. Moser, A. Neuhold, J. Novák, S. A. Ponomarenko, Q. Shen, C. Teichert, G. Hlawacek, P. Puschnig, C. A. -Draxl, R. Resel, and D. M. de Leeuw, *J. Phys. Chem. C* **115**, 22925 (2011).
- <sup>14</sup>S. V. Morozov, K. S. Novoselov, M. I. Katsnelson, F. Schedin, L. A. Ponomarenko, D. Jiang, and A. K. Geim, *Phys. Rev. Lett.* **97**, 016801 (2006).
- <sup>15</sup>A. Fasolino, J. H. Los, and M. I. Katsnelson, *Nature Mater.* **6**, 858 (2007).
- <sup>16</sup>V. Geringer, M. Liebmann, T. Echtermeyer, S. Runte, M. Schmidt, R. Rückamp, M. C. Lemme, and M. Morgenstern, *Phys. Rev. Lett.* **102**, 076102 (2009).
- <sup>17</sup>A. Locatelli, K. R. Knox, D. Cvetko, T. O. Menteş, M. A. Nino, S. Wang, M. B. Yilmaz, P. Kim, R. M. Osgood, Jr., and A. Morgante, *ACS Nano* **4**, 4879 (2010).
- <sup>18</sup>A. Sinitskii, D. V. Kosynkin, A. Dimiev, and J. M. Tour, *ACS Nano* **4**, 3095 (2010).
- <sup>19</sup>W. Bao, F. Miao, Z. Chen, H. Zhang, W. Jang, C. Dames, and C. N. Lau, *Nat. Nanotechnol.* **4**, 562 (2009).
- <sup>20</sup>C.-C. Chen, W. Bao, J. Theiss, C. Dames, C. N. Lau, and B. Cronin, *Nano Lett.* **9**, 4172 (2009).
- <sup>21</sup>Z. Wang and M. Devel, *Phys. Rev. B* **83**, 125422 (2011).